ORIGINAL RESEARCH

Impairment of Fatty Acid Oxidation in Alveolar Epithelial Cells Mediates Acute Lung Injury

Huachun Cui[1], Na Xie[1], Sami Banerjee[1], Jing Ge[2], Sijia Guo[1,3], and Gang Liu[1]

[1]Division of Pulmonary, Allergy, and Critical Care Medicine, Department of Medicine, University of Alabama at Birmingham, Birmingham, Alabama; [2]Department of Geriatrics and Institute of Geriatrics, Union Hospital, Tongji Medical College, Huazhong University of Science and Technology, Wuhan, China; and [3]Department of Pulmonary, Allergy, and Critical Care Medicine, the Second Affiliated Hospital, Tianjin University of Traditional Chinese Medicine, Tianjin, China

ORCID ID: 0000-0003-2615-131X (G.L.).

Abstract

Profound impairment in cellular oxygen consumption, referred to as cytopathic dysoxia, is one of the pathological hallmarks in the lungs of patients with pathogen-induced acute lung injury (ALI). However, the underlying mechanism for this functional defect remains largely unexplored. In this study, we found that primary mouse alveolar epithelial cells (AECs) conducted robust fatty acid oxidation (FAO). More importantly, FAO was strikingly impaired in AECs of mice with LPS-induced ALI. The metabolic deficiency in these cells was likely due to decreased expression of key mediators involved in FAO and mitochondrial bioenergenesis, such as peroxisome proliferator–activated receptor γ coactivator (PGC)-1α, carnitine palmitoyltransferase 1A, and medium-chain acyl-CoA dehydrogenase (CAD). We found that treatment of alveolar epithelial line MLE-12 cells with BAL fluids from mice with ALI decreased FAO, and this effect was largely replicated in MLE-12 cells treated with the proinflammatory cytokine TNF-α, which was consistent with downregulations of PGC-1α, carnitine palmitoyltransferase 1A, long-chain CAD, and medium-chain CAD in the same treated cells. Furthermore, we found that the BAL fluids from ALI mice and TNF-α inhibited MLE-12 bioenergenesis and promoted cell apoptosis. In delineation of the role of FAO in ALI *in vivo*, we found that conditional ablation of AEC PGC-1α aggravated LPS-induced ALI. In contrast, fenofibrate, an activator of the PPAR-α/PGC-1α cascade, protected mice from this pathology. In summary, these data suggest that FAO is essential to AEC bioenergenesis and functional homeostasis. This study also indicates that FAO impairment–induced AEC dysfunction is an important contributing factor to the pathogenesis of ALI.

Keywords: alveolar epithelial cell; fatty acid oxidation; acute lung injury; peroxisome proliferator–activated receptor γ coactivator-1α

Among pathological hallmarks of acute lung injury (ALI), there is a profound impairment in cellular oxygen consumption, called cytopathic dysoxia, and a proinflammatory cytokine storm produced by immune cells, such as neutrophils and macrophages (1–7). The cytopathic dysoxia is thought to be resulted from abnormalities of mitochondria, as they are the primary oxygen-consuming subcellular organelles (1, 3, 4, 8–11). Persistent defects in mitochondrial bioenergetics leads to cell death, which contributes to the pathogenesis of ALI (8, 12). However, the molecular mechanism underlying the cytopathic dysoxia in ALI is largely unknown.

Alveolar epithelial cells (AECs), together with pulmonary microvascular endothelial cells, form the blood–air barrier that is essential to gas exchange and pulmonary fluid homeostasis (13–15). Dysfunctions of AECs have been well recognized to be important contributing factors to ALI pathologies, such as destruction of alveolar barriers, accumulation of pulmonary fluids, and decreased production of surfactants (13–17). However, the mechanisms underlying these AEC abnormalities are incompletely understood.

(Received in original form April 25, 2018; accepted in final form September 4, 2018)

This work was supported by National Institutes of Health grants HL135830 and HL114470.

Author Contributions: H.C. and N.X. contributed equally to this work; H.C. and G.L. designed the study; H.C., N.X., S.B., J.G., S.G., and G.L. performed the experiments and/or analyzed the data; G.L. supervised the study; H.C., N.X., and G.L. wrote the manuscript.

Correspondence and requests for reprints should be addressed to Gang Liu, M.D., Ph.D., Division of Pulmonary, Allergy, and Critical Care Medicine, Department of Medicine, University of Alabama at Birmingham, 901 19th Street South, BMR II 233, Birmingham, AL 35294. E-mail: gangliu@uabmc.edu.

Am J Respir Cell Mol Biol Vol 60, Iss 2, pp 167–178, Feb 2019

Originally Published in Press as DOI: 10.1165/rcmb.2018-0152OC on September 5, 2018
Internet address: www.atsjournals.org

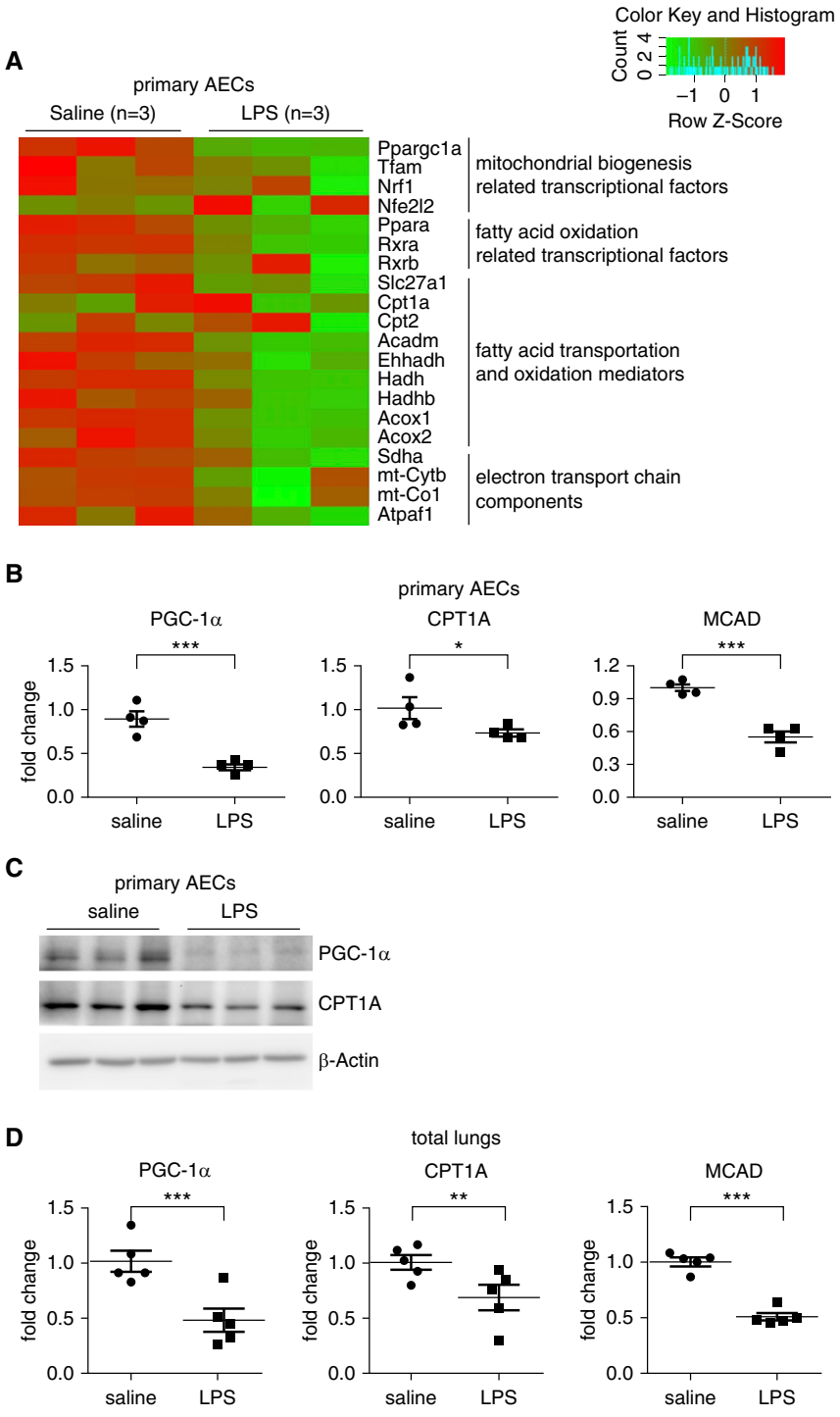

Figure 1. Key regulatory mediators involved in fatty acid oxidation (FAO) and mitochondrial bioenergenesis are downregulated in alveolar epithelial cells (AECs) of acute lung injury (ALI) mice. (*A*) Primary AECs were purified from mice that were instilled intratracheally with saline or LPS (2 mg/kg) for 24 hours. Total RNAs were isolated and RNA sequencing analysis performed. Heat map of gene expression of regulators and mediators related to FAO and mitochondrial biogenesis and energenesis are presented. (*B* and *C*) The expression of the indicated genes in AECs was determined by real-time PCR (*B*) and Western blotting (*C*). (*A–C*) $n = 3$ for the saline and LPS groups, respectively; mean ± SEM; $^{*}P < 0.05$, $^{***}P < 0.001$. (*D*) The expression of the indicated genes in total lungs was determined by real-time PCR. $n = 5$ for the saline and LPS groups, respectively; mean ± SEM; $^{**}P < 0.01$, $^{***}P < 0.001$. PGC-1α = peroxisome proliferator–activated receptor γ coactivator-1α.

Glucose and fatty acids are the primary bioenergetic sources for mammalian cells. Whereas almost all types of cells prefer glucose, skeletal myocytes, cardiomyocytes, hepatocytes, and adipocytes mainly oxidize fatty acids in mitochondria to fuel ATP production, a process termed fatty acid oxidation (FAO) (18–22). Nevertheless, it has been unclear what bioenergetic nutrients AECs use in resting state, and how these metabolic programs are affected under stressful settings.

The pivotal mitochondrial regulator, peroxisome proliferator–activated receptor (PPAR) γ coactivator (PGC)-1α, promotes FAO by inducing critical mediators in this metabolic process, including carnitine palmitoyltransferase I (CPT1), a key enzyme that mediates transportation of fatty acids across mitochondrial membrane into matrix (18, 23, 24). Once inside the mitochondria, fatty acids undergo a series of reactions, including acyl-CoA dehydrogenase (CAD)–mediated dehydrogenation, hydration, oxidation, and thiolysis for acetyl-CoA production to fuel the citric acid cycle (19, 25). Very long chain fatty acids are first oxidized in peroxisomes (peroxisomal FAO), with acyl-coenzyme A oxidase 1 being the first enzyme. This process results in length reduction of the very long chain fatty acids before they can be processed in mitochondria (26).

In this study, we found that AECs conduct robust FAO, and this metabolic program was remarkably reduced in AECs of mice with LPS-induced ALI. We found that impairment of FAO diminished AEC bioenergenesis and rendered the cells susceptible to apoptosis. Our data suggest that FAO impairment leads to AEC dysfunctions that contributes to ALI pathogenesis.

Methods

Reagents

Ultrapure LPS from *Escherichia coli* O111: B4, palmitic acid, fenofibrate, and fatty acid–free BSA were purchased from Sigma-Aldridge. Etomoxir (ETO) was from Cayman Chemical. Mouse recombinant TNF-α was from Peprotech.

Cell Line

The mouse AEC line, MLE-12, and HEK-293T cells were purchased from the

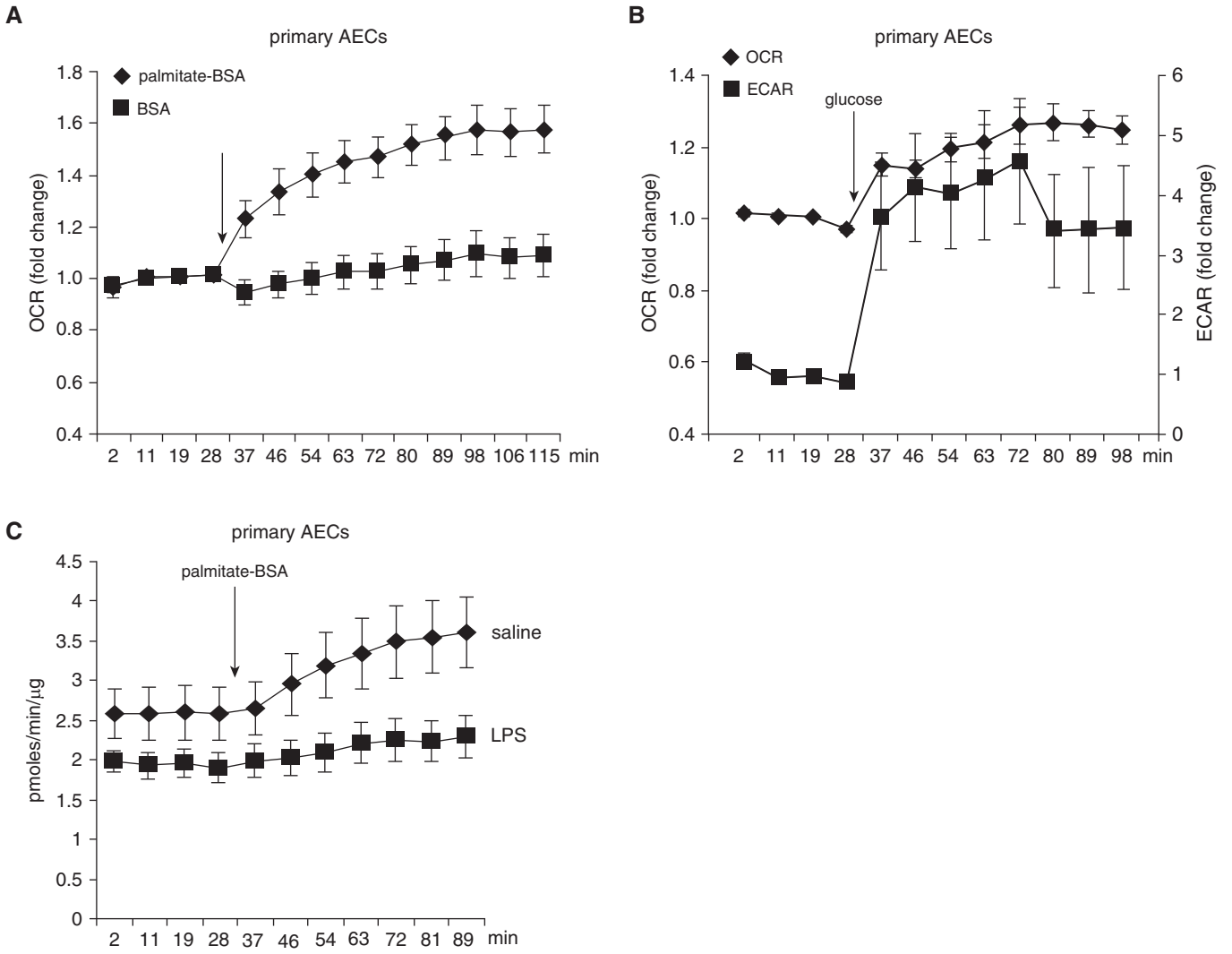

Figure 2. AECs use both glucose and fatty acids, and FAO is impaired in AECs of mice with LPS-induced ALI. (*A*) Primary AECs were seeded in Seahorse XF-24 microplates and incubated with substrate-limited media for 3 hours. Basal oxygen consumption rate (OCR) was then recorded before BSA or palmitate-BSA (final concentration: 150 μM) was injected into the wells. After injection, OCR was continuously monitored until it reached the maximum value. $n = 4$ per group; mean ± SEM. (*B*) Primary AECs were seeded in Seahorse XF-24 microplates and incubated with extracellular acidification rate (ECAR) media for 1 hour. Basal OCR and ECAR were then recorded before glucose (final concentration: 10 mM) was injected into the wells. After injection, OCR and ECAR were continuously monitored until they reached the maximum values. $n = 3$ per group; mean ± SEM. (*C*) Primary AECs purified from saline or intratracheal LPS–treated mice were seeded in Seahorse XF-24 microplates and incubated with substrate-limited media for 3 hours. Basal OCR was then recorded before palmitate-BSA was injected into the wells. After injection, OCR was continuously monitored until it reached the maximum value. OCR values were normalized to total protein content of the cellular extract from each well. $n = 4$ mice per group; mean ± SEM.

American Type Culture Collection and cultured according to the their instructions.

Generation of Conditional Knockout Mice with Ablation of PGC-1α in AECs

To generate AEC PGC-1$\alpha^{-/-}$ mice, *Ppargc1a* floxed mice (PGC-1$\alpha^{fl/fl}$; stock #009666; The Jackson Laboratory) were cross-bred with *Sftpc-CreER*^{T2} mouse line (stock #028054; The Jackson Laboratory) to obtain mice with *Ppargc1a*$^{fl/fl}$/*Sftpc-CreER*$^{T2+/+}$ or *Ppargc1a*$^{fl/fl}$/*Sftpc-CreER*$^{T2+/-}$ genotype. To induce AEC PGC-1α deletion, these mice (at age 10 wk) were injected intraperitoneally with tamoxifen dissolved in corn oil (75 mg/kg body weight) once a day for 5 days. *PGC-1α*$^{fl/fl}$ mice that received the same dosage of tamoxifen were used as controls. At 3 days after the last intraperitoneal injection, the mice were used for ALI experiments. C57BL/6 male mice (8 wk old) were also purchased from The Jackson Laboratory. The animal protocol was approved by the UAB Institutional Animal Care and Use Committee.

RNA Sequencing Assay

RNA sequencing (RNA-seq) was performed by Arraystar Inc. RNA-seq data were submitted to the Gene Expression Omnibus and are unrestrictedly accessible with accession number GSE109913 (available

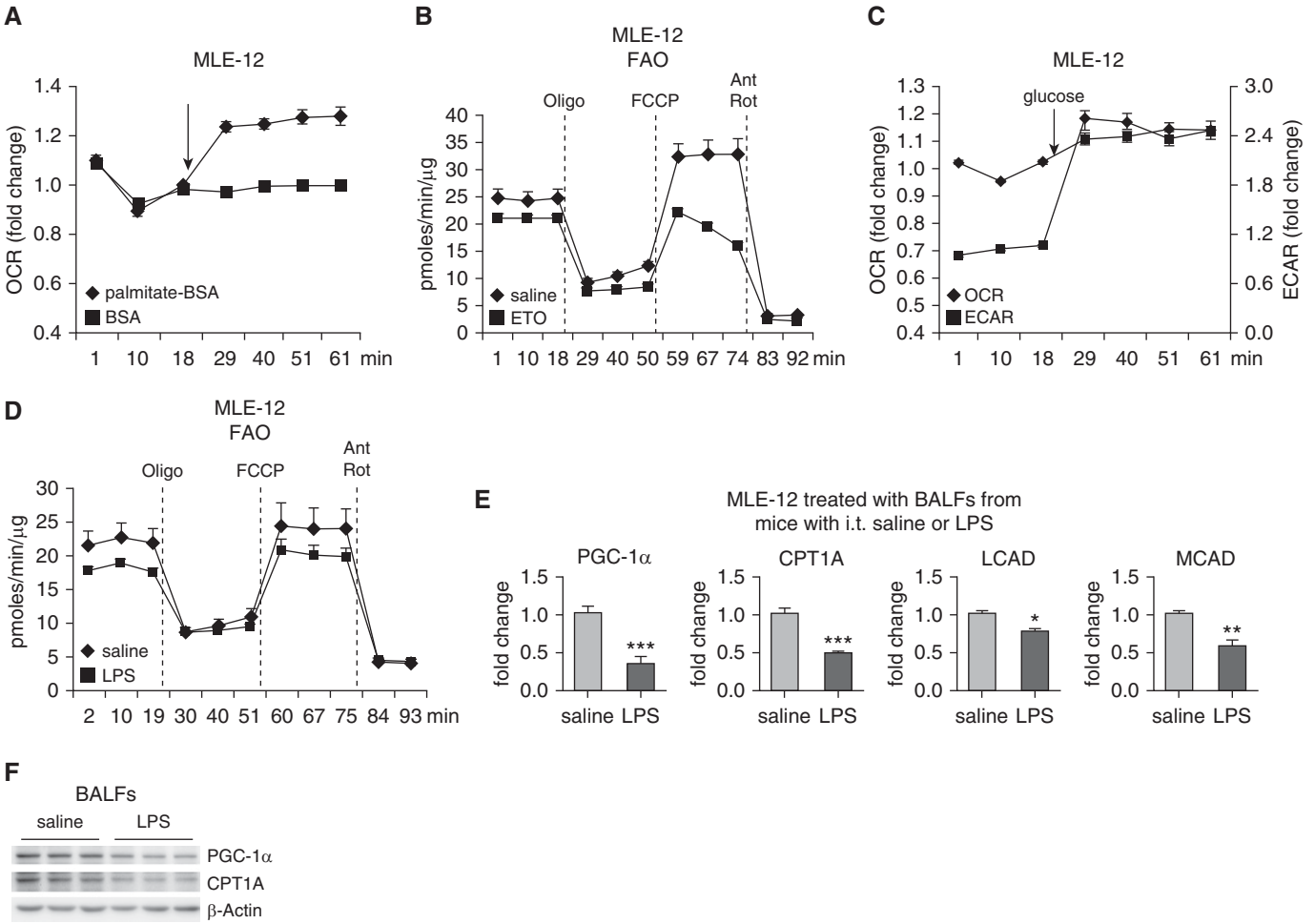

Figure 3. Alveolar epithelial line MLE-12 cells use fatty acids, and FAO is impaired in MLE-12 treated with BAL fluid (BALF) from ALI mice. (*A*) Alveolar epithelial line MLE-12 cells were seeded in Seahorse XF-24 microplates and incubated with substrate-limited media for 12 hours. Basal OCR was then recorded before BSA or palmitate-BSA was injected into the wells. After injection, OCR was continuously monitored until it reached the maximum value. $n = 5$ or 6 for the palmitate-BSA or BSA group; mean ± SEM. (*B*) MLE-12 cells were seeded in Seahorse XF-24 microplates and treated with saline or 100 μM etomoxir (ETO) for 1 hour. The media were then replaced with FAO assay media supplemented with 150 μM palmitate-BSA and cultured for 1 hour, followed by sequential treatments with 3 μg/ml oligomycin (Oligo), 6 μM FCCP, and 1 μM rotenone (Rot) and 0.5 μM antimycin A (Ant). Real-time OCR was recorded. $n = 6$ or 5 for the saline or ETO group; mean ± SEM. (*C*) MLE-12 cells were seeded in Seahorse XF-24 microplates and incubated with ECAR media for 1 hour. Basal OCR and ECAR were then recorded before glucose (final concentration: 10 mM) was injected into the wells. After injection, OCR and ECAR were continuously monitored until they reached the maximum values. $n = 7$; mean ± SEM. (*D*) MLE-12 cells were seeded in Seahorse XF-24 microplates and treated for 16 hours with BALF pooled from five mice instilled intratracheally with saline or LPS. The media were then replaced with FAO assay media supplemented with 150 μM palmitate-BSA and cultured for 1 hour, followed by sequential treatments with 3 μg/ml oligomycin, 6 μM FCCP, and 1 μM Rot and 0.5 μM Ant. Real-time OCR was recorded. $n = 6$ per group; mean ± SEM. (*E–F*) MLE-12 cells were incubated for 16 hours with BALFs from mice instilled intratracheally with saline or LPS for 24 hours. The mRNA (*E*) and/or protein (*F*) levels of indicated genes were determined by real-time PCR and Western blotting. (*E*) $n = 3$; mean ± SD; $^*P < 0.05$, $^{**}P < 0.01$, $^{***}P < 0.001$ compared with saline group. FCCP = Carbonyl cyanide 4-(trifluoro) methoxyphenylhydrazone.

online at https://www.ncbi.nlm.nih.gov/geo/query/acc.cgi?acc=GSE109913).

Establishment and Evaluation of LPS-induced ALI

Mice were instilled intratracheally LPS (2 mg/kg in 50 μl saline). At 24 hours after treatment, mice were killed and the following assays were performed to evaluate severity of lung injury: determination of BAL fluid (BALF) leukocyte numbers and protein concentrations; determination of BALF and lung proinflammatory cytokine levels; lung histological evaluation.

Isolation of Mouse AECs

Lungs were minced and incubated with digestion buffer (Hank's Balanced Salt Solution, containing 0.1% type I collagenase, 0.1% dispase II, and 0.01% DNase I) for 1 hour at 37°C. Single-cell suspensions were prepared by passing the lung digestions through a 40-μm mesh size cell strainer. The cells were then pelleted and red blood cell lysed. Primary AECs were obtained by subjecting the single-cell suspensions to a negative selection by incubation with biotin-conjugated anti-CD16/32, -CD45, -CD31, -CD90, -Ter119, and -PDGFR-α antibodies (BD

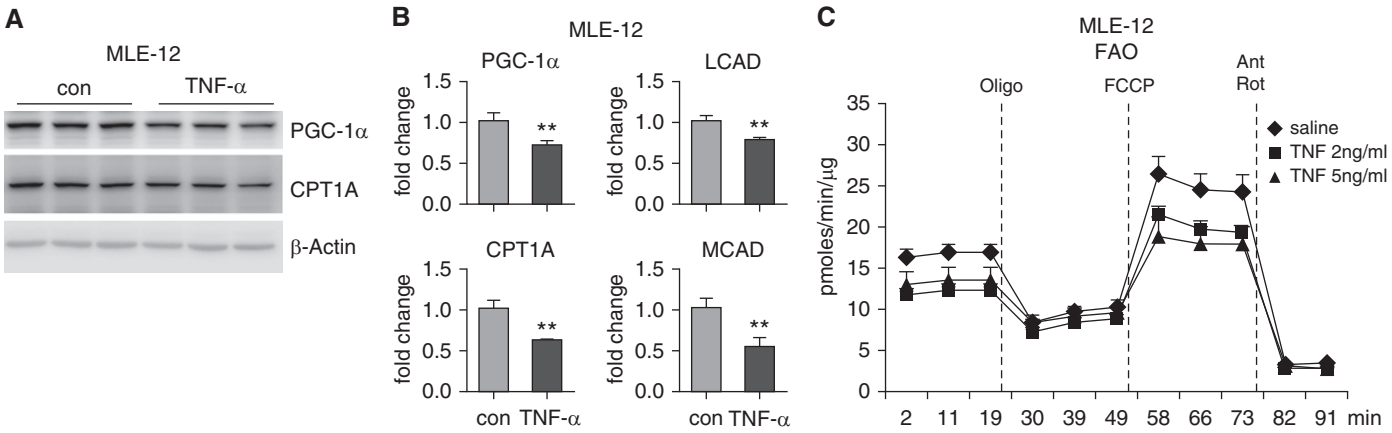

Figure 4. Proinflammatory cytokine TNF-α inhibits FAO in AECs. (*A* and *B*) MLE-12 cells were treated for 16 hours with 2 ng/ml recombinant mouse TNF-α. The protein (*A*) and/or mRNA (*B*) levels of indicated genes were determined by Western blotting and real-time PCR. $^{**}P < 0.01$ compared with control group. (*C*) MLE-12 cells were seeded in Seahorse XF-24 microplates and treated with 2 ng/ml or 5 ng/ml mouse TNF-α in Opti-MEM overnight. The media were then replaced with FAO assay media supplemented with 150 μM palmitate-BSA and cultured for 1 hour, followed by sequential treatments with 3 μg/ml oligomycin, 6 μM FCCP, and 1 μM rotenone and 0.5 μM antimycin A. Real-time oxygen consumption rate was recorded. $n = 6$ per group; mean ± SEM. con = control; MEM = Eagle's minimum essential medium.

Biosciences), and streptavidin-conjugated magnetic beads (Promega) to deplete myeloid and lymphoid cells, endothelial cells, and mesenchymal fibroblasts.

Determination of Intracellular ATP Levels

Intracellular ATP levels were determined using Luminescent ATP Detection Assay Kit (Abcam) according to the manufacturer's instructions.

Determination of AEC Apoptosis

AECs were incubated with annexin V–FITC and propidium iodide from an Apoptosis Detection Kit (BD Biosciences) according to the manufacturer's instructions, and cell apoptosis was analyzed by flow cytometry. Percentages of annexin V and propidium iodide–positive cells were determined by flow cytometry.

Real-Time PCR

mRNA levels were determined by real-time PCR using SYBR Green Master Mix Kit (Roche). Primer sequences were: mouse tubulin α1: sense, 5′ GGATGCTGCCA ATAACTATGCTCGT 3′, antisense, 5′ GCCAAAGCTGTGGAAAACCAAGAAG 3′; mouse PGC-1α: sense, 5′ CCTC ACACCAAACCCACAGAAAACA 3′, antisense, 5′ GGTGACTCTG GGGTCAGAGGAAGAG 3′; mouse CPT1A: sense, 5′ GGGATATAG AGAGGAGGACCCTGAGG 3′, antisense, 5′ GCGTTTATGCCTATCTTGCTGTTTTT 3′; mouse medium-chain CAD (MCAD): sense, 5′ TGCCAGAGAGGAGATTATCCCCGT 3′, antisense, 5′ CACCCATACGCCAA CTCTTCGGTA 3′; mouse long-chain CAD (LCAD): sense, 5′ GCCTAACAGAGCCCT CGAGTGGAT 3′, antisense, 5′ ATTGGC GTCTTGGCAAAGACAGTG 3′; mouse PPAR-α: sense, 5′ CACCTTCTACG CTCCCGACCCATC 3′, antisense, 5′ GGAACCAAGCCCCTCCATCCACTG 3′. To calculate fold change in the expression of these genes, ΔCt = cycle threshold (Ct) of tubulin − Ct of individual genes was first obtained. ΔΔCt = ΔCt of treated groups − Δ Ct of untreated control groups was then obtained. Fold change was calculated as $2^{\Delta\Delta Ct}$, with control groups as onefold.

Western Blotting

Western blotting was performed as previously described (27). Mouse anti–β-actin antibody was from Sigma-Aldrich. Mouse anti–PGC-1α antibody was from EMD Millipore. Rabbit anti-CPT1A antibody was from Proteintech. Rabbit anti-cleaved caspase-3 was from Cell Signaling Technology.

Lentivirus Preparation

The full-length cDNA of mouse PGC-1α was purchased from Dharmacon. The open reading frame (ORF) of PGC-1α was amplified by PCR and subcloned into the BamH1 and Not1 sites of lentiviral vector pCDH-EF1-MCS (System Biosciences). HEK-293T cells were co-transfected with pCDH-EF1-MCS or pCDH-EF1–PGC-1α and the third generation packaging constructs. Cells were cultured according to the manufacturer's instructions (System Biosciences). Media that contained lentivirus were collected at Days 3 and 4 after transfection. For transduction, MLE-12 cells were incubated with the lentivirus-containing media (50% of total culture media).

ELISA

Levels of proinflmammatory cytokines were determined using DuoSet ELISA development kits (R&D Systems) according to the manufacturer's instructions.

Real-Time Cell Metabolism Assay

XF-24 Extracellular Flux Analyzer (Seahorse Bioscience) was used for real-time recordings of oxygen consumption rate (OCR) and extracellular acidification rate (ECAR). To record real-time OCR with cells fed with BSA or palmitate-BSA, primary AECs or MLE-12 cells were seeded in Seahorse XF-24 microplates and incubated with substrate-limited media (Seahorse Bioscience) for 3 hours (primary AECs) or 24 hours (MLE-12). Basal OCR was then recorded before BSA or palmitate-BSA (final concentration: 150 μM) was injected into the wells according to the manufacturer's manual. After injection, OCR was continuously monitored until it reached the maximum value. To record real-time OCR and ECAR with cells fed with glucose, primary AECs or MLE-12 cells were seeded

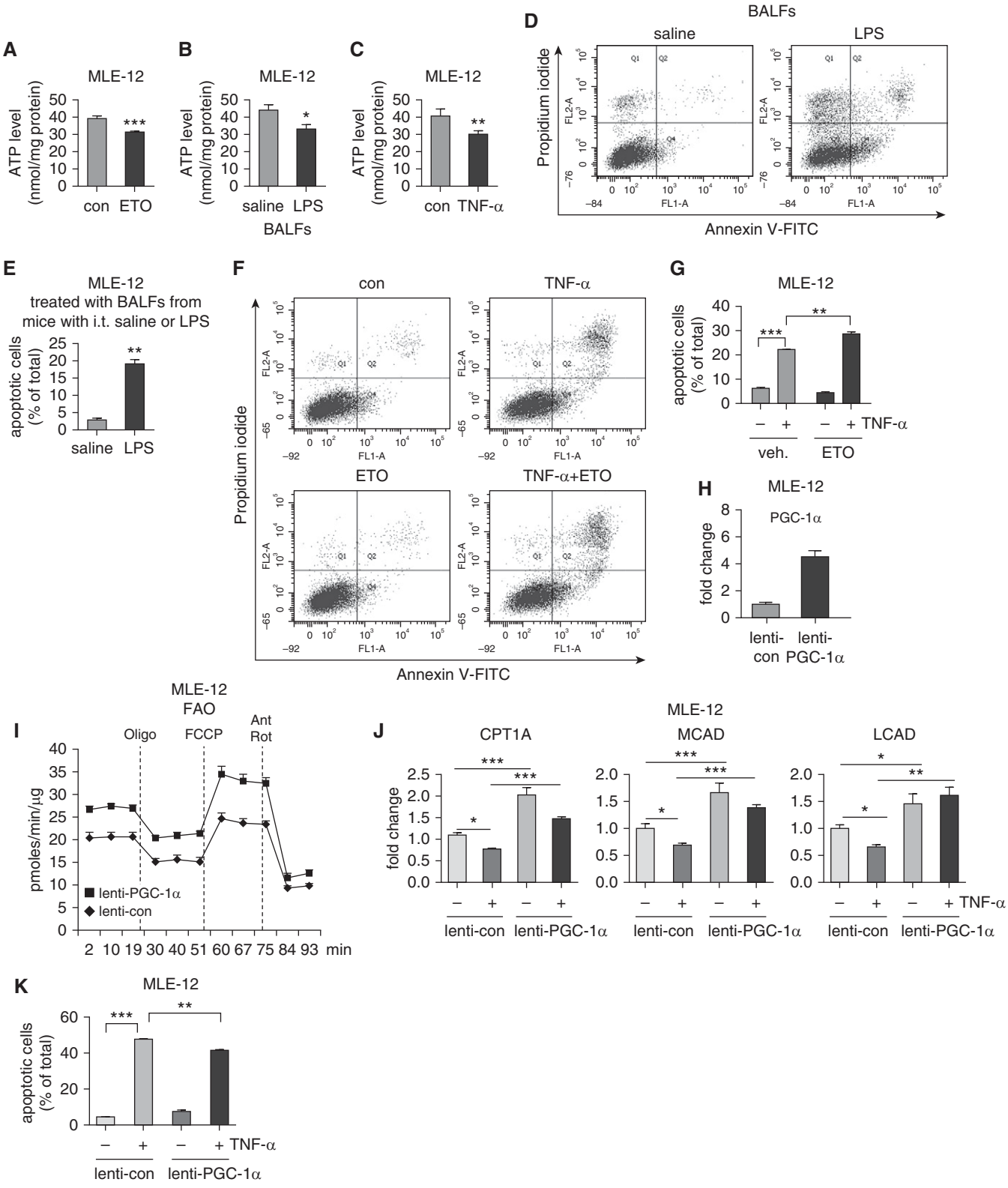

Figure 5. Blocking FAO decreases intracellular ATP levels and promotes AEC apoptosis. (*A–C*) MLE-12 cells were treated for 16 hours with 100 μM ETO (*A*), BALFs from mice instilled intratracheally with saline or LPS (*B*), or 2 ng/ml mouse TNF-α (*C*). Intracellular ATP levels were determined using Luminescent ATP Detection Assay Kit. $n = 4$; mean ± SD; $^{*}P < 0.05$, $^{**}P < 0.01$, $^{***}P < 0.001$ compared with respective control group. (*D* and *E*) MLE-12 cells were treated for 16 hours with BALFs from mice instilled intratracheally with saline or LPS. The cells were harvested and incubated with

in Seahorse XF-24 microplates and incubated with ECAR media for 1 hour. Basal OCR and ECAR were then recorded before glucose (final concentration: 10 mM) was injected into the wells. After injection, OCR and ECAR were continuously monitored until they reached the maximum values. To determine the effects of TNF-α on FAO, MLE-12 cells were seeded in Seahorse XF-24 microplates and treated with TNF-α in Opti-MEM media (Life Technologies) overnight. The media were then replaced with FAO assay media (111 mM NaCl, 4.7 mM KCl, 1.25 mM $CaCl_2$, 2 mM $MgSO_4$, 1.2 mM NaH_2PO_4, 2.5 mM glucose, 0.5 mM carnitine, and 5 mM HEPES, supplemented with 150 μM palmitate-BSA; Seahorse Bioscience) and cultured for 1 hour, followed by sequential treatments with 3 μg/ml oligomycin, 6 μM FCCP, and 1 μM rotenone and 0.5 μM antimycin A. Real-time OCR was recorded. To determine the effects of BALFs from ALI mice on FAO, MLE-12 cells were seeded in Seahorse XF-24 microplates and treated with BALFs pooled from five mice instilled intratracheally with saline or LPS for 16 hours (4 × 1 ml Opti-MEM media lavage/mouse). The BALFs were then replaced with FAO assay media supplemented with 150 μM palmitate-BSA and cultured for 1 hour, followed by sequential treatments with 3 μg/ml oligomycin, 6 μM FCCP, and 1 μM rotenone and 0.5 μM antimycin A. Real-time OCR was recorded. Values of OCR and ECAR were normalized with protein content of cellular extract from each well.

Statistical Analysis

One-way ANOVA, followed by the Bonferroni test, was used for multiple group comparisons. The Student's *t* test was used for comparison between two groups. *P* less than 0.05 was considered statistically significant.

Results

Key Regulatory Mediators Involved in FAO and Mitochondrial Bioenergenesis are Downregulated in AECs of ALI Mice

To delineate the molecular mechanisms underlying AEC dysfunctions in ALI, we performed RNA-seq analysis on primary AECs purified from mice with LPS-induced ALI and control animals. Standouts among those downregulated in the AECs of ALI lungs were a number of key mediators involved in FAO and mitochondrial bioenergenesis, such as PGC-1α, CPT1, and MCAD (18, 23, 24, 28), indicative of functional impairments with the subcellular activities (Figure 1A). The reduced expression of some of these genes in the AECs of ALI lungs was confirmed by real-time PCR as well as Western blot analysis (Figures 1B and 1C). In addition, we found that these mediators in the whole lungs of ALI mice were downregulated to levels comparable to those in the AECs (Figure 1D), suggesting that AECs are the primary targets of the metabolic dysregulations. These data also indicate that impaired FAO and mitochondrial bioenergenesis in AECs may contribute to the pathogenesis of ALI.

AECs Use both Glucose and Fatty Acids

Despite the implication of the impaired FAO and mitochondrial bioenergenesis in ALI pathology, metabolic programs in AECs have not been clearly delineated. There has been even less evidence of if or how individual metabolisms in AECs participate in the pathogenesis of pulmonary disorders associated with dysfunctions of these cells, including ALI. To characterize metabolic programs in AECs, we initially focused on the mitochondrial oxidations of two core nutrients (e.g., fatty acids and glucose) by using Seahorse Analyzer. As shown in Figure 2A, there was gradually increased OCR in primary mouse AECs while being fed with fatty acids in the form of palmitate conjugated to BSA. In contrast, OCR remained unchanged when the cells were supplied with BSA (Figure 2A). These data suggest that AECs readily use fatty acids that undergo mitochondrial oxidation. In addition, we found that AECs also demonstrated a robust glycolytic program. However, a large share of the program was channeled to produce the end-product lactate, instead of supplying the mitochondrial respiration, as evidenced by a spike in ECAR, accompanied by a moderate increase of OCR when the cells were fed with glucose (Figure 2B). Taken together, these data suggest that FAO constitutes an essential part of the metabolic programs in AECs.

FAO Is Impaired in AECs of Mice with LPS-induced ALI

To determine the role of AEC FAO in ALI, we isolated primary AECs from mice treated intratracheally with saline or LPS and measured real-time OCR in these cells. As shown in Figure 2C, although AECs from saline-treated mice demonstrated rapidly elevated OCR upon being fed with fatty acids, AECs from mice with LPS-induced ALI showed little response to fatty acids, indicative of markedly impaired FAO in these cells. Taken together, these data suggest that FAO impairment may mediate AEC dysfunctions in ALI.

Alveolar Epithelial Line MLE-12 Cells Use Fatty Acids, and FAO Is Impaired in MLE-12 Treated with BALF from ALI Mice

We have shown that primary mouse AECs conduct robust FAO, and this metabolic program is markedly diminished in AECs of

Figure 5. (Continued). annexin V–FITC and propidium iodide (PI). Cell apoptosis was analyzed by flow cytometry (*D*). Percentages of apoptotic cells were plotted (*E*). (*F* and *G*) MLE-12 cells were pretreated for 1 hour with 100 μM ETO, followed by incubation with 2 ng/ml mouse TNF-α for 16 hours. Cell apoptosis was analyzed by flow cytometry (*F*). Percentages of apoptotic cells were plotted (*G*). (*D–G*) $n = 3$; mean ± SD; $^{**}P < 0.01$, $^{***}P < 0.001$. (*H*) MLE-12 cells were transduced with control lentivirus or lentivirus that expressed mouse PGC-1α. Levels of PGC-1α were determined 1 day after transduction. (*I*) MLE-12 cells were transduced with control lentivirus or lentivirus that expressed mouse PGC-1α. The cells were then plated in Seahorse XF-24 microplates overnight. The media were then replaced with FAO assay media supplemented with 150 μM palmitate-BSA and cultured for 1 hour, followed by sequential treatments with 3 μg/ml oligomycin, 6 μM FCCP, and 1 μM Rot and 0.5 μM Ant. Real-time oxygen consumption rate was recorded. $n = 6$ per group; mean ± SEM. (*J*) MLE-12 cells were transduced with control lentivirus or lentivirus that expressed mouse PGC-1α. The cells were treated with TNF-α overnight. The expression of the indicated genes were determined by real-time PCR. $n = 3$; mean ± SD; $^{*}P < 0.05$, $^{**}P < 0.01$, $^{***}P < 0.001$. (*K*) The cell transduction and treatment were conducted as in *J*, and annexin V–FITC and PI assay performed. Percentages of apoptotic cells were plotted. $n = 4$; mean ± SD; $^{**}P < 0.01$, $^{***}P < 0.001$.

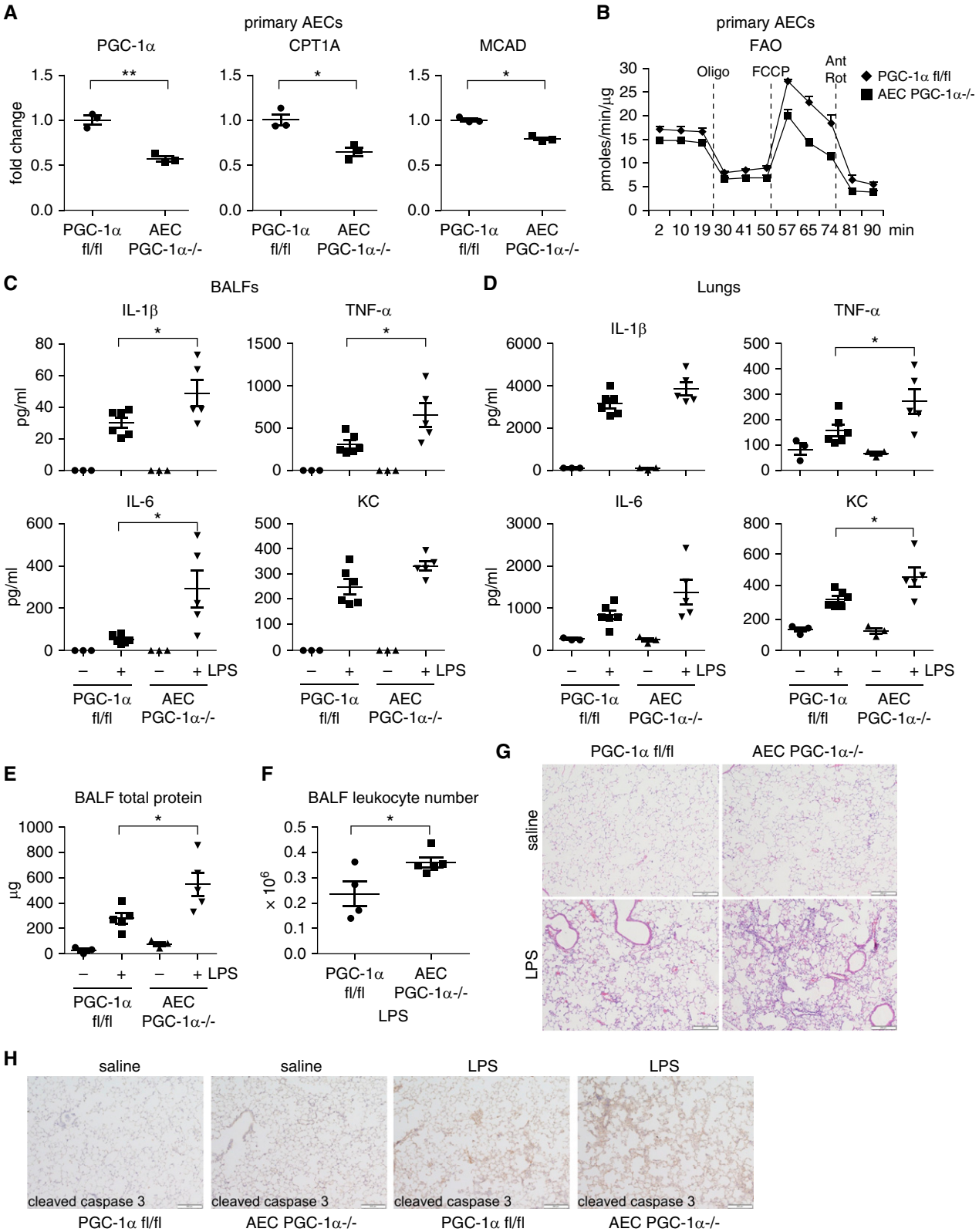

Figure 6. Ablation of AEC PGC-1α aggravates LPS-induced ALI. (*A*) AECs were purified from the control PGC-1α$^{fl/fl}$ and AEC PGC-1α$^{-/-}$ mice and levels of the indicated genes determined. $n = 3$; mean ± SEM; $^{*}P < 0.05$, $^{**}P < 0.01$. (*B*) Mice were treated with tamoxifen as in *A*. AECs were purified, seeded in Seahorse microplates in FAO assay media supplemented with 150 μM palmitate-BSA and cultured for 1 hour, followed by sequential treatments with 3 μg/ml oligomycin, 6 μM FCCP, and 1 μM Rot and 0.5 μM Ant. Real-time OCR was recorded. $n = 2$ per group. (*C* and *D*) The control PGC-1α$^{fl/fl}$ and AEC

ALI lungs. To delineate the regulatory mechanism and the functional outcome of FAO deficiency in AECs, we chose a well-established mouse AEC line, MLE-12, to serve as a cellular model for further investigations. We first examined fatty acid metabolism in these cells, and found that MLE-12 cells, just like the primary AECs, effectively used fatty acids through mitochondrial oxidation (Figure 3A). As expected, FAO in MLE-12 cells was notably diminished by the specific inhibitor of CPT1A, ETO (Figure 3B). In addition, we found that, also similar to that in the primary AECs, the glycolytic program in MLE-12 cells was largely ushered to lactate production, with a moderate destination for mitochondrial oxidation (Figure 3C). These data suggest that the metabolic programs in MLE-12 are comparable to those in the primary AECs.

To determine if the metabolic pathology in AECs of ALI mice could be replicated *in vitro*, we treated MLE-12 cells with BALFs from ALI mice, and found that OCR with FAO assay was diminished in these cells (Figure 3D), suggestive of an impairment on FAO. The compromised OCR in MLE-12 treated with BALFs from ALI lungs could be attributed to downregulations of PGC-1α, CPT1A, LCAD, and MCAD in the cells (Figures 3E and 3F). Taken together, these findings suggest that FAO impairment in AECs of ALI lungs is an effect of local pathological settings.

Proinflammatory Cytokine TNF-α Inhibits FAO in AECs

We showed the FAO inhibitory activity of BALFs from ALI mice, we next reasoned that proinflammatory cytokines in the BALFs from these mice accounted for the downregulation of the key mediators in FAO and mitochondrial bioenergenesis and the ensuing inhibition of FAO. To test this hypothesis, we treated MLE-12 cells with proinflammatory cytokine, TNF-α, and found that the expression of PGC-1α, CPT1A, LCAD, and MCAD was all decreased in the TNF-α–treated cells (Figures 4A and 4B). Concordantly, we found that TNF-α markedly inhibited OCR in MLE-12 cells (Figure 4C), suggestive of a compromised FAO. Taken together, these data suggest that the proinflammatory cytokines in the inflamed lungs lead to FAO defects in the AECs through downregulating the critical mediators in this metabolic program.

FAO Participates in AEC Bioenergenesis and Promotes AEC Survival

As cellular bioenergenesis is critical to cell survival and functional homeostasis, we next asked if FAO was essential to the bioenergetic output of AECs. We treated MLE-12 cells with ETO and found that ETO significantly decreased intracellular ATP levels (Figure 5A), indicative of a critical contribution of FAO to the AEC bioenergenesis. Furthermore, we found that MLE-12 treated with BALFs from ALI mice or TNF-α demonstrated markedly reduced intracellular ATP levels (Figures 5B and 5C), consistent with their inhibitions of FAO in the cells. Taken together, our data suggest that proinflammatory cytokines in the inflamed lungs impair AEC bioenergenesis through downregulating FAO in these cells.

Bioenergetic defect leads to cellular dysfunctions and death (8, 12). In addition, AEC apoptosis is one of the pathological hallmarks of ALI lungs. This body of information led to the hypothesis that the compromised FAO in AECs participated in apoptosis of these cells in injured lungs. To test this, we treated MLE-12 cells with BALFs from ALI mice, and found that these cells demonstrated significantly elevated apoptosis as compared with those treated with normal BALFs (Figures 5D and 5E). We also found that TNF-α induced MLE-12 apoptosis (Figures 5F and 5G). More importantly, TNF-α–induced MLE-12 apoptosis was significantly enhanced by the FAO inhibitor, ETO. Notably, although ETO inhibited ATP production, it alone failed to cause MLE-12 cell death, suggesting that the compromised bioenergenesis due to FAO impairment is not a sufficient, but a susceptible factor which aggravates AEC dysfunction in the inflamed lung, an environment enriched with proapoptotic inducers, such as TNF-α and reactive oxygen species. To further define the role of FAO in regulating TNF-α–induced AEC apoptosis, we directly overexpressed the master FAO regulator, PGC-1α, in MLE-12 cells through lentiviral delivery of recombinant DNA constructs (Figure 5H). Likely as a result of overexpression, there was a markedly augmented OCR in these cells (Figure 5I), which was also consistent with the upregulation of the PGC-1α–dependent, critical FAO mediators, CPT1A, MCAD, and LCAD (Figure 5J). More importantly, we found that overexpression of PGC-1α demonstrated a very consistent, though modest protection from TNF-α–induced apoptosis (Figure 5K). Taken together, these findings suggest that the proinflammatory cytokines in the inflamed lungs promote AEC apoptosis by inhibiting FAO in these cells.

Ablation of AEC PGC-1α Aggravates LPS-induced ALI

PGC-1α is a master regulator of FAO and mitochondrial bioenergenesis (18, 23, 24, 29). Given our findings that AECs in ALI lungs demonstrated markedly reduced expression of PGC-1α and impaired FAO, we reasoned that AEC PGC-1α was critical to the fitness of these cells and participated in ALI pathology. To test this hypothesis, we established conditional knockout mice with ablation of PGC-1α in AECs (AEC PGC-1$\alpha^{-/-}$). We first validated that

Figure 6. (Continued). PGC-1$\alpha^{-/-}$ mice were instilled intratracheally with saline or LPS (2 mg/kg in 50 μl saline). At 24 hours after treatment, the mice were killed and BALF (0.5 ml for 3 times/mouse) and lungs collected. BALF was centrifuged to collect supernatants and cell pellets. Red blood cells in the cell pellets were lysed. The whole lungs were homogenized in 3-ml protein extraction buffer. Levels of indicated proinflammatory cytokines in BALF (*C*) and lung extracts (*D*) were determined by ELISA. (*E* and *F*) Total protein levels (*E*) and leukocyte numbers (*F*) in the BALFs. *$P < 0.05$. (*G*) Lungs of experiments similar to *C* were fixed with 10% neutral-buffered formalin and tissue slides prepared. Hematoxylin and eosin staining was performed. (*H*) Lungs of experiments similar to *C* were fixed and tissue slides prepared. Immunohistochemistry (IHC) assays for cleaved caspase 3 were performed. Rabbit IgG was used as IHC negative control. (*G* and *H*) Original magnification ×100; scale bars: 200 μm.

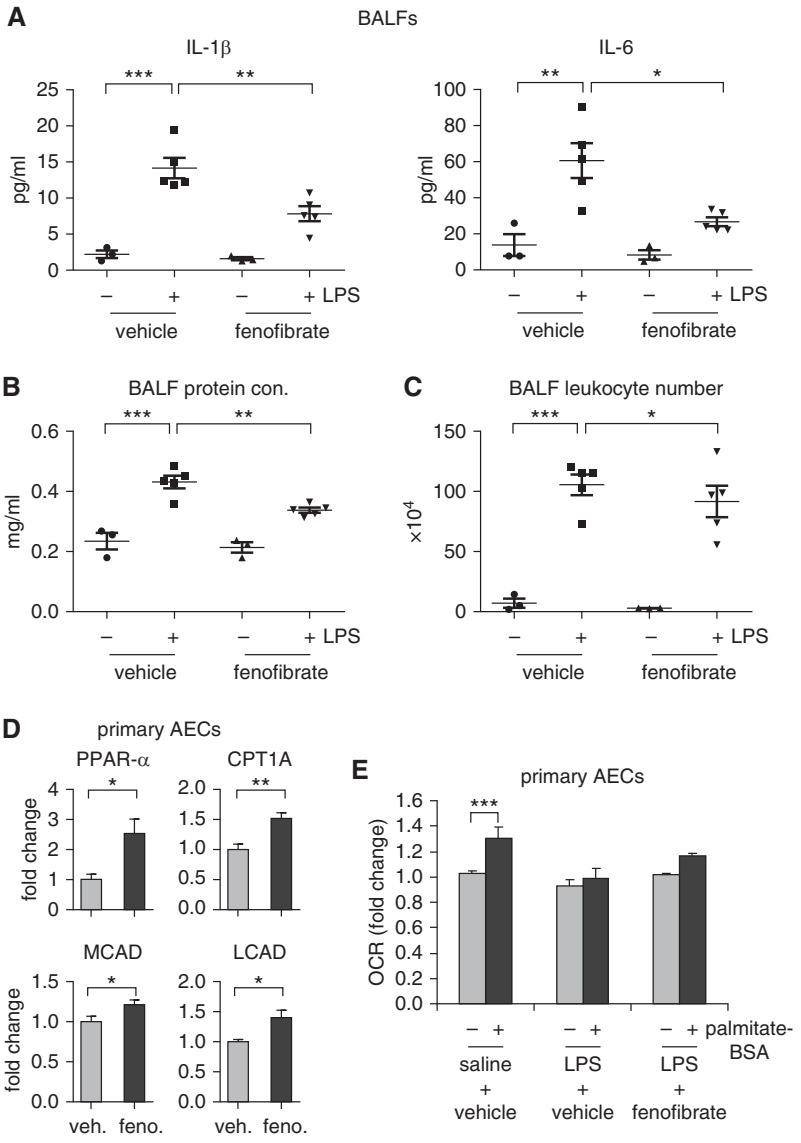

Figure 7. The activator of PGC-1α/peroxisome proliferator–activated receptor-α cascade, fenofibrate, attenuates LPS-induced ALI in mice. C57BL/6 mice (8 wk old) were instilled intratracheally with saline or LPS (2 mg/kg in 50 μl saline). At 4 hours after the intratracheal treatment, the mice were injected intraperitoneally with vehicle or fenofibrate (100 mg/kg body weight). At 24 hours after saline or LPS instillation, the mice were killed and BALF (0.5 ml for 3 times/mouse) collected. BALF was centrifuged to collect supernatants and cell pellets. Red blood cells in the cell pellets were lysed. Levels of indicated proinflammatory cytokines (*A*), protein concentrations (*B*), and total leukocyte numbers (*C*) in BALF was determined. (*A–C*) $n = 3, 5, 3, 5$ mice, respectively; mean ± SEM; $^{*}P < 0.05$, $^{**}P < 0.01$, $^{***}P < 0.001$. (*D*) Primary AECs were purified from mice injected intraperitoneally with vehicle or fenofibrate. Levels of the indicated genes in the cells were determined. $n = 3$; mean ± SEM; $^{*}P < 0.05$, $^{**}P < 0.01$. (*E*) Primary AECs purified from saline- or LPS-instilled mice injected intraperitoneally with vehicle or fenofibrate were seeded in Seahorse XF-24 microplates and incubated with substrate-limited media for 3 hours. Basal OCR was then recorded before BSA or palmitate-BSA was injected into the wells. After injection, OCR was continuously recorded until stable levels were reached. Fold change in average OCR values were plotted. $n = 4, 4, 2$; $^{***}P < 0.001$.

PGC-1α level was reduced, as expected, in AECs from these mice after induction of ablation of the floxed alleles by tamoxifen (Figure 6A). The expression of PGC-1α–dependent CPT1A and MCAD was also decreased in these cells (Figure 6A). Consistent with the role of these mediators in FAO, we found that OCR with FAO assay in AEC PGC-$1\alpha^{-/-}$ cells was markedly decreased compared with that in AEC PGC-$1\alpha^{fl/fl}$ controls (Figure 6B). We found that there was no obvious inflammation or injury in the lungs of saline-treated AEC PGC-$1\alpha^{-/-}$ mice (Figures 6C–6E), indicative of nonessential function of AEC PGC-1α to pulmonary homeostasis. However, compared with the wild-type PGC-$1\alpha^{fl/fl}$ mice, AEC PGC-$1\alpha^{-/-}$ animals demonstrated aggravated LPS-induced lung injury, as evidenced by increased levels of proinflammatory cytokines in BALFs and lungs, and augmented lung protein leaks and leukocyte infiltrations (Figures 6C–6G). Furthermore, we found that there was enhanced AEC apoptosis in LPS-treated AEC PGC-$1\alpha^{-/-}$ mice, indicated by more evident staining of cleaved caspase 3 in the AECs of these animals (Figure 6H), consistent with the elevated susceptibility to apoptosis of MLE-12 cells *in vitro* when FAO was impaired. Taken together, these data suggest that PGC-1α is essential to AEC survival and homeostasis in the setting of ALI.

The Activator of PPAR-α/PGC-1α Cascade, Fenofibrate, Attenuates LPS-induced ALI in Mice

As PGC-1α acts together with PPAR-α to regulate FAO (30), we examined the effect of the PPAR-α agonist, fenofibrate, on LPS-induced ALI. As shown in Figures 7A–7C, administration of fenofibrate 4 hours after intratracheal LPS significantly attenuated LPS-induced ALI, as evidenced by reduced proinflammatory cytokine levels, leukocyte numbers, and protein levels in BALFs from these mice. To determine if the protective effect of fenofibrate was associated with FAO, we examined the expression of those FAO mediators in AECs purified from mice treated with this drug, and found that the levels of PPARα CPT1A, MCAD, and LCAD were significantly increased in these cells compared with those from vehicle-treated animals (Figure 7D). Consistent with the elevated expression of these FAO mediators, there was a trend of reversal of the impaired FAO in AECs from ALI mice that received fenofibrate (Figure 7E). Taken together, these data in general support the notion that augmentation of AEC FAO is beneficial in ALI, although we caution against a stretched interpretation because fenofibrate is likely to have PPAR-α/PGC-1α– or FAO-independent activities.

Nevertheless, these findings suggest that FAO could become a novel therapeutic target for treating this lung disorder.

Discussion

Although AEC dysfunctions have been well recognized to have critical contributions to ALI pathologies (15, 31), there is a scarcity of studies that investigate the underlying mechanisms from the standpoint of cellular metabolism. We provide the first line of evidence that AECs effectively conduct FAO. Our data show that AEC FAO has a critical role in maintaining the functional homeostasis of these cells. Our study thus establishes the dysregulation of FAO as a metabolic phenotype for ALI.

Focusing of this study on AEC FAO was literally guided by our RNA-seq analysis that revealed the reduced expression of important mediators in FAO and mitochondrial bioenergenesis. Although scientifically rationalized, we are aware of the fact that other metabolic programs, such as those involving amino acids, may also participate in AEC dysfunctions in ALI. In addition, not all mediators associated with metabolic programs are affected at the transcriptional level, which is the only information that the RNA-seq analysis could reveal. Nevertheless, this study opens a new avenue of investigations into interactions of metabolism and cellular functions, particularly in AECs, in lung disorders.

We have found that AEC PGC-1α is significantly downregulated in ALI lungs. Furthermore, ablation of AEC PGC-1α aggravated LPS-induced ALI. Although PGC-1α is a key regulator of FAO, it has a myriad of additional regulatory functions, such as controlling mitochondrial biogenesis, oxidative phosphorylation, gluconeogenesis, and glycogenolysis, whereby it regulates the catabolism of other nutrients, including glucose (32, 33). Therefore, the effect of PGC-1α downregulation on AEC bioenergenesis may not be entirely caused by the impaired FAO, but also by diminished glucose oxidation in these cells. This speculation is, in general, supported by previous studies showing that there is elevated glycolysis in inflamed lungs, a metabolic reprogramming response that is normally used to compensate for insufficient mitochondrial oxidative phosphorylation activity (34). However, the exact contributions of fatty acids and glucose oxidation to AEC bioenergenesis may only be determined with carbon isotope tracing techniques. Along similar lines, augmented LPS-induced lung injury in mice with ablation of AEC PGC-1α may be derived from AEC dysfunction caused by defective mitochondrial oxidative phosphorylation that undermines both fatty acids and glucose catabolism.

We showed that BAFL from ALI lungs decreased the expression of the key mediators in FAO and mitochondrial bioenergenesis, including PGC-1α, CPT1A, MCAD, and LCAD. We also found that TNF-α, one of the predominant proinflammatory cytokines in ALI lungs, achieved a similar effect. Although it is certain that the downregulation is at least at the transcriptional level, the regulatory mechanism remains unknown. Given that our data suggest that the impairment in FAO in AECs is an effect secondary to the production of inflammatory cytokines in ALI, the delineation of how proinflammatory signaling events inhibit the expression of these key mediators may help to identify the means to uncouple lung inflammation and AEC dysfunction, which could become novel therapeutics to treat this disorder.

We have shown that FAO is significantly impaired in AECs of ALI lungs, and the defective FAO leads to diminished bioenergenesis and apoptosis in these cells. These findings solidly implicate FAO in AEC dysfunction and ALI pathogenesis. However, other types of pulmonary cells, such as endothelial cells and macrophages, may also conduct active FAO. Indeed, there has been plenty of evidence that FAO is critical to the development of an antiinflammatory M2 phenotype in macrophages (35, 36). In addition, FAO was recently shown to be required for endothelial cell proliferation (37). Given that the dysfunction of these two types of cells also demonstrate pivotal participation in ALI pathogenesis by causing alveolar–capillary barrier destruction and cytokine storm (38–41), it is reasonable to speculate that some therapeutic efficacies of boosting FAO in the lung in ALI may be derived from FAO-augmented antiinflammation and proproliferation in pulmonary macrophages and microvascular endothelial cells, respectively. These two events have been shown to be immensely beneficial in the treatment of experimental ALI in animal models (42–44). Therefore, it remains a very interesting direction forward to delineate the role of FAO in pulmonary macrophages and endothelial cells in the pathogenesis of ALI. ■

Author disclosures are available with the text of this article at www.atsjournals.org.

References

1. Brealey D, Brand M, Hargreaves I, Heales S, Land J, Smolenski R, *et al*. Association between mitochondrial dysfunction and severity and outcome of septic shock. *Lancet* 2002;360:219–223.
2. Loiacono LA, Shapiro DS. Detection of hypoxia at the cellular level. *Crit Care Clin* 2010;26:409–421. (Table of contents).
3. Schumacker PT, Samsel RW. Oxygen delivery and uptake by peripheral tissues: physiology and pathophysiology. *Crit Care Clin* 1989;5:255–269.
4. Singer M. Mitochondrial function in sepsis: acute phase versus multiple organ failure. *Crit Care Med* 2007;35(9 suppl):S441–S448.
5. Tunceroglu H, Shah A, Porhomayon J, Nader ND. Biomarkers of lung injury in critical care medicine: past, present, and future. *Immunol Invest* 2013;42:247–261.
6. Matthay MA, Ware LB, Zimmerman GA. The acute respiratory distress syndrome. *J Clin Invest* 2012;122:2731–2740.
7. Standiford TJ, Ward PA. Therapeutic targeting of acute lung injury and acute respiratory distress syndrome. *Transl Res* 2016;167: 183–191.
8. Schumacker PT, Gillespie MN, Nakahira K, Choi AM, Crouser ED, Piantadosi CA, *et al*. Mitochondria in lung biology and pathology: more than just a powerhouse. *Am J Physiol Lung Cell Mol Physiol* 2014;306:L962–L974.
9. Agrawal A, Mabalirajan U. Rejuvenating cellular respiration for optimizing respiratory function: targeting mitochondria. *Am J Physiol Lung Cell Mol Physiol* 2016;310:L103–L113.
10. Creery D, Fraser DD. Tissue dysoxia in sepsis: getting to know the mitochondrion. *Crit Care Med* 2002;30:483–484.

11. Crouser ED, Julian MW, Blaho DV, Pfeiffer DR. Endotoxin-induced mitochondrial damage correlates with impaired respiratory activity. *Crit Care Med* 2002;30:276–284.
12. Tang PS, Mura M, Seth R, Liu M. Acute lung injury and cell death: how many ways can cells die? *Am J Physiol Lung Cell Mol Physiol* 2008;294: L632–L641.
13. Martin TR, Hagimoto N, Nakamura M, Matute-Bello G. Apoptosis and epithelial injury in the lungs. *Proc Am Thorac Soc* 2005;2:214–220.
14. Perl M, Chung CS, Lomas-Neira J, Rachel TM, Biffl WL, Cioffi WG, *et al*. Silencing of Fas, but not caspase-8, in lung epithelial cells ameliorates pulmonary apoptosis, inflammation, and neutrophil influx after hemorrhagic shock and sepsis. *Am J Pathol* 2005;167:1545–1559.
15. Bhattacharya J, Matthay MA. Regulation and repair of the alveolar–capillary barrier in acute lung injury. *Annu Rev Physiol* 2013;75: 593–615.
16. Budinger GR, Mutlu GM, Urich D, Soberanes S, Buccellato LJ, Hawkins K, *et al*. Epithelial cell death is an important contributor to oxidant-mediated acute lung injury. *Am J Respir Crit Care Med* 2011;183: 1043–1054.
17. Maidji E, Kosikova G, Joshi P, Stoddart CA. Impaired surfactant production by alveolar epithelial cells in a SCID-hu lung mouse model of congenital human cytomegalovirus infection. *J Virol* 2012; 86:12795–12805.
18. Houten SM, Wanders RJ. A general introduction to the biochemistry of mitochondrial fatty acid β-oxidation. *J Inherit Metab Dis* 2010;33:469–477.
19. Carracedo A, Cantley LC, Pandolfi PP. Cancer metabolism: fatty acid oxidation in the limelight. *Nat Rev Cancer* 2013;13:227–232.
20. Sebastián D, Guitart M, García-Martínez C, Mauvezin C, Orellana-Gavaldà JM, Serra D, *et al*. Novel role of FATP1 in mitochondrial fatty acid oxidation in skeletal muscle cells. *J Lipid Res* 2009;50: 1789–1799.
21. Lopaschuk GD, Jaswal JS. Energy metabolic phenotype of the cardiomyocyte during development, differentiation, and postnatal maturation. *J Cardiovasc Pharmacol* 2010;56:130–140.
22. Lee J, Choi J, Scafidi S, Wolfgang MJ. Hepatic fatty acid oxidation restrains systemic catabolism during starvation. *Cell Reports* 2016;16:201–212.
23. Fucho R, Casals N, Serra D, Herrero L. Ceramides and mitochondrial fatty acid oxidation in obesity. *FASEB J* 2017;31:1263–1272.
24. Qu Q, Zeng F, Liu X, Wang QJ, Deng F. Fatty acid oxidation and carnitine palmitoyltransferase I: emerging therapeutic targets in cancer. *Cell Death Dis* 2016;7:e2226.
25. O'Neill LA, Kishton RJ, Rathmell J. A guide to immunometabolism for immunologists. *Nat Rev Immunol* 2016;16:553–565.
26. Zeng J, Deng S, Wang Y, Li P, Tang L, Pang Y. Specific inhibition of acyl-CoA oxidase-1 by an acetylenic acid improves hepatic lipid and reactive oxygen species (ROS) metabolism in rats fed a high fat diet. *J Biol Chem* 2017;292:3800–3809.
27. Xie N, Tan Z, Banerjee S, Cui H, Ge J, Liu RM, *et al*. Glycolytic reprogramming in myofibroblast differentiation and lung fibrosis. *Am J Respir Crit Care Med* 2015;192:1462–1474.
28. Supruniuk E, Mikłosz A, Chabowski A. The implication of PGC-1α on fatty acid transport across plasma and mitochondrial membranes in the insulin sensitive tissues. *Front Physiol* 2017;8:923.
29. Chau BN, Xin C, Hartner J, Ren S, Castano AP, Linn G, *et al*. MicroRNA-21 promotes fibrosis of the kidney by silencing metabolic pathways. *Sci Transl Med* 2012;4:121ra18.
30. Kang HM, Ahn SH, Choi P, Ko YA, Han SH, Chinga F, *et al*. Defective fatty acid oxidation in renal tubular epithelial cells has a key role in kidney fibrosis development. *Nat Med* 2015;21:37–46.
31. Matthay MA, Zemans RL. The acute respiratory distress syndrome: pathogenesis and treatment. *Annu Rev Pathol* 2011;6:147–163.
32. Lindholm D, Eriksson O, Mäkelä J, Belluardo N, Korhonen L. PGC-1α: a master gene that is hard to master. *Cell Mol Life Sci* 2012;69: 2465–2468.
33. Kadlec AO, Chabowski DS, Ait-Aissa K, Gutterman DD. Role of PGC-1α in vascular regulation: implications for atherosclerosis. *Arterioscler Thromb Vasc Biol* 2016;36:1467–1474.
34. Sadiku P, Willson JA, Dickinson RS, Murphy F, Harris AJ, Lewis A, *et al*. Prolyl hydroxylase 2 inactivation enhances glycogen storage and promotes excessive neutrophilic responses. *J Clin Invest* 2017;127: 3407–3420.
35. Huang SC, Everts B, Ivanova Y, O'Sullivan D, Nascimento M, Smith AM, *et al*. Cell-intrinsic lysosomal lipolysis is essential for alternative activation of macrophages. *Nat Immunol* 2014;15: 846–855.
36. Mills EL, O'Neill LA. Reprogramming mitochondrial metabolism in macrophages as an anti-inflammatory signal. *Eur J Immunol* 2016; 46:13–21.
37. Schoors S, Bruning U, Missiaen R, Queiroz KC, Borgers G, Elia I, *et al*. Fatty acid carbon is essential for dNTP synthesis in endothelial cells. *Nature* 2015;520:192–197.
38. Millar FR, Summers C, Griffiths MJ, Toshner MR, Proudfoot AG. The pulmonary endothelium in acute respiratory distress syndrome: insights and therapeutic opportunities. *Thorax* 2016;71:462–473.
39. Mehta D, Ravindran K, Kuebler WM. Novel regulators of endothelial barrier function. *Am J Physiol Lung Cell Mol Physiol* 2014;307: L924–L935.
40. Aggarwal NR, King LS, D'Alessio FR. Diverse macrophage populations mediate acute lung inflammation and resolution. *Am J Physiol Lung Cell Mol Physiol* 2014;306:L709–L725.
41. Tsushima K, King LS, Aggarwal NR, De Gorordo A, D'Alessio FR, Kubo K. Acute lung injury review. *Intern Med* 2009;48:621–630.
42. Stevens TC, Ochoa CD, Morrow KA, Robson MJ, Prasain N, Zhou C, *et al*. The *Pseudomonas aeruginosa* exoenzyme Y impairs endothelial cell proliferation and vascular repair following lung injury. *Am J Physiol Lung Cell Mol Physiol* 2014;306:L915–L924.
43. Morrison TJ, Jackson MV, Cunningham EK, Kissenpfennig A, McAuley DF, O'Kane CM, *et al*. Mesenchymal stromal cells modulate macrophages in clinically relevant lung injury models by extracellular vesicle mitochondrial transfer. *Am J Respir Crit Care Med* 2017;196: 1275–1286.
44. Guo Z, Wen Z, Qin A, Zhou Y, Liao Z, Liu Z, *et al*. Antisense oligonucleotide treatment enhances the recovery of acute lung injury through IL-10–secreting M2-like macrophage-induced expansion of $CD4^+$ regulatory T cells. *J Immunol* 2013;190:4337–4348.